



Morphology, Dielectric and EMI Shielding Characteristics of Graphene Nanoplatelets, Montmorillonite Nanoclay and Titanium Dioxide Nanoparticles Reinforced Polyvinylidene fluoride Nanocomposites

A. Harish Kumar¹ · M. Basheer Ahamed¹ · Kalim Deshmukh² · Mohamed Sheik Sirajuddeen¹

Received: 26 October 2020 / Accepted: 20 December 2020 / Published online: 4 January 2021
© The Author(s), under exclusive licence to Springer Science+Business Media, LLC part of Springer Nature 2021

Abstract

Herein, flexible polyvinylidene fluoride (PVDF) nanocomposite films reinforced with different concentrations of graphene nanoplatelets (GNPs), montmorillonite (MMT) nanoclay and titanium dioxide (TiO₂) nanoparticles (NPs) were prepared using a simple and low-cost solution casting method. The surface morphology of PVDF/GNPs/TiO₂/MMT nanocomposites and the interaction between PVDF, GNPs, TiO₂ NPs and MMT nanofillers was examined using Fourier transform infrared (FTIR) spectroscopy, X-ray diffraction (XRD) and field emission scanning electron microscopy (FESEM) techniques. The dielectric properties of the prepared nanocomposite films were evaluated using a frequency response impedance analyzer in the frequency range from 50 Hz to 20 MHz at various temperatures. The electromagnetic interference (EMI) shielding effectiveness (SE) of PVDF/GNPs/TiO₂/MMT nanocomposites was measured in the Ku-band region (12–18 GHz) and the maximum SE of 12.6 dB was obtained for nanocomposites with GNPs-2.5%, MMT-1% and TiO₂-11.5%. Considering the excellent EMI shielding performance, these nanocomposites can have promising applications in smart electronics and flexible devices.

Keywords PVDF · GNPs · TiO₂ NPs · MMT · EMI shielding · SEM

1 Introduction

The boundless and explosive growth in the electrical, electronics and telecommunication industries have enabled the substantial generation of unwanted electromagnetic (EM) pollution which is known as electromagnetic interference, EMI [1, 2]. The EM radiation emitted from the source generates considerable heat emissions thereby affecting the normal operation of electronic equipment and also leads to the malfunctioning of the neighbouring instruments [3, 4]. The EM radiations are also hazardous and can have serious effects on human health. Therefore, EMI shielding materials are essential to shield or to reduce the effect of this

undesired pollution [5, 6]. The shielding material must have high absorption, high reflection and very less or negligible transmittance of EM radiation [3–8]. Traditionally, metals have been frequently used for EMI shielding because of their excellent conductivity, but they exhibit several drawbacks such as poor processability, high density, narrow absorption bandwidth, corrosive nature and heavyweight, etc. [5–9]. Therefore, nowadays, researchers are gradually replacing metal-based materials with flexible and low-cost polymer nanocomposites (PNCs) for the development of novel and efficient EMI shielding materials.

Recently, PNCs have attracted great attraction in different research fields because of their lightweight, easy processability, flexibility, low cost and excellent properties which can be tailored as per specific application needs [10–15]. Based on the intended applications, different types of conducting nanoparticles (NPs), metal oxides, metal and fibers or clay nanopowders can be added to a polymer matrix to achieve effective and homogeneous dispersion within the polymer matrix to obtain significant enhancement in the desired properties [16–20]. Furthermore, studies have shown that integrating two or more fillers into the polymer matrix

✉ M. Basheer Ahamed
basheerahamed@crecident.education

¹ Department of Physics, B. S. Abdur Rahman Crescent Institute of Science and Technology, Vandalur, Chennai 600048, India

² New Technologies-Research Centre, University of West Bohemia, 30100 Plzeň, Czech Republic

can be more resourceful in achieving enhanced EMI SE [21–24]. Polyvinylidene fluoride (PVDF) is one of the most frequently investigated polymers especially used for preparing flexible PNCs. It is a semi-crystalline, ferroelectric polymer with good thermal stability, high melting point, excellent mechanical and dielectric properties [25, 26]. PVDF has mainly four crystal polymorphic phases namely α , β , γ and δ . Among them, the α -phase is the most common and stable polymorph [25–27]. The phase behaviour of PVDF has been studied extensively where the β -phase of PVDF was found to have good functionality, high tensile toughness, excellent piezoelectric and pyroelectric properties and good processability [28–30]. Thus, PVDF is a very promising polymeric material in the field of EMI shielding nanocomposites.

Graphene is an outstanding two-dimensional (2D) material comprising sp^2 bonded carbon atoms arranged in a honeycomb structure [31]. Graphene exhibits excellent optical, electrical, thermal and tensile properties [31, 32]. These intriguing properties of graphene have triggered enormous interest in its implementation in a vast number of applications such as supercapacitors [33], fuel cells [34], photonics and optoelectronics [35] and lithium-ion batteries [36]. Graphene nanoplatelets (GNPs) are composed of single or few-layer graphene with thicker graphite [37]. GNPs exhibit a planar structure with excellent properties such as large aspect ratio, lightweight, excellent electrical and thermal conductivity and mechanical strength [37, 38]. Furthermore, GNPs based PNCs have demonstrated improved flexural and tribological properties [39, 40]. Montmorillonite (MMT) consists of an intercalated structure with an expanded inter-layer spacing of layered aluminosilicates [41]. MMT nanoclay particles are frequently used as filler materials that can be efficiently dispersed within the polymer matrix. Studies have revealed enhanced structural and tribological properties of PNCs when MMT was dispersed into the PVDF matrix [42, 43]. Titanium dioxide (TiO_2) NPs have been the most widely used nanofiller in the development of PNCs owing to their promising properties such as good chemical stability, high refractive index, good dielectric properties and excellent corrosion resistance [44, 45]. TiO_2 NPs reinforced PNCs have been shown to display considerable antibacterial activity, mechanical, dielectric and flame retardant properties [46–48].

The EMI shielding properties of various PNCs or hybrid materials have been investigated by several authors owing to their superior electrical properties. For example; Sabira et al. [49] developed 20 μm thick, flexible, and mechanically stable PVDF/graphene nanocomposite films and observed an EMI SE value of 47 dB in the X-band frequency region. Hamidinejad et al. [50] fabricated high-density polyethylene/GNPs composite foams by supercritical fluid treatment and physical foaming process. The resultant composite foam exhibited an EMI SE of 31.6 dB at 19 vol% GNPs loading.

In another study, Vyas and Chandra [23] reported poly (vinylidene fluoride-*co*-hexafluoropropylene) (PVDF-HFP) nanocomposite films comprising multi-walled carbon nanotubes (MWCNTs) as an electron-conducting network and barium titanate ($BaTiO_3$) as ferroelectric ceramic nanofiller. The resultant composite exhibited EMI SE value of ~ 81 dB in the X-band (8–12 GHz) region. These studies demonstrate that several factors such as size, shape, structure, thickness, filler content, conductivity and percolation threshold are responsible for achieving enhanced EMI SE of PNCs [38, 49–51]. Also, increasing the nanofiller content into the polymer matrix leads to an improved conductivity and low leakage current of the nanocomposites thereby providing enhanced EMI SE values [23]. Thus, with this background knowledge, in the present work, GNPs, MMT and TiO_2 NPs reinforced PVDF nanocomposites were prepared and their dielectric and EMI shielding properties were examined.

2 Experimental Procedure

2.1 Materials

PVDF powder was purchased from Pragati Plastics PVT Ltd., New Delhi, India. GNPs (Type 1) of carbon content 99.5%, thickness 6–8 nm and average particle size of 15 μm and MMT nanopowder of average particle size 80–150 nm and elemental compositions SiO_2 -65%, Al_2O_3 -15%, Fe_2O_3 -1.3%, Ti_2O -0.19%, K_2O -1.3%, Na_2O -0.65%, CaO -3.31% and MgO -0.99% was purchased from Sisco Research Laboratories (SRL) Pvt. Ltd., Mumbai, India. TiO_2 NPs employed in this study was AEROXIDE hydrophilic fumed TiO_2 P25 with an average particle size of 21 nm, high specific surface area of 50 ± 15 m^2/g and crystallographic composition of 80% anatase and 20% rutile was supplied by Degussa, Germany. *N, N*-dimethylformamide (DMF) with >99% purity used as the solvent in the present study was supplied by Qualigens Fine Chemicals, Mumbai, India.

2.2 Preparation of PVDF/GNPs/MMT/ TiO_2 Nanocomposite Films

The PVDF/GNPs/MMT/ TiO_2 nanocomposite films were prepared using the solution casting method as illustrated in Fig. 1. The feed compositions used for the preparation of nanocomposite films are shown in Table 1. Initially, the desired amount of PVDF powder was dissolved in 20 ml DMF by heating at 70 $^\circ C$ in the hot air oven until a clear solution was obtained. Meanwhile, GNPs were dispersed in 15 ml DMF and sonicated using an ultrasonic bath (Model: LMUC-2, capacity 2 l, ultrasonic frequency 40 kHz, heating ambient to 80 $^\circ C$, timer 0 to 60 min, power supply 220 V, 50 Hz) for 1 h. Similarly, the TiO_2 NPs and MMT

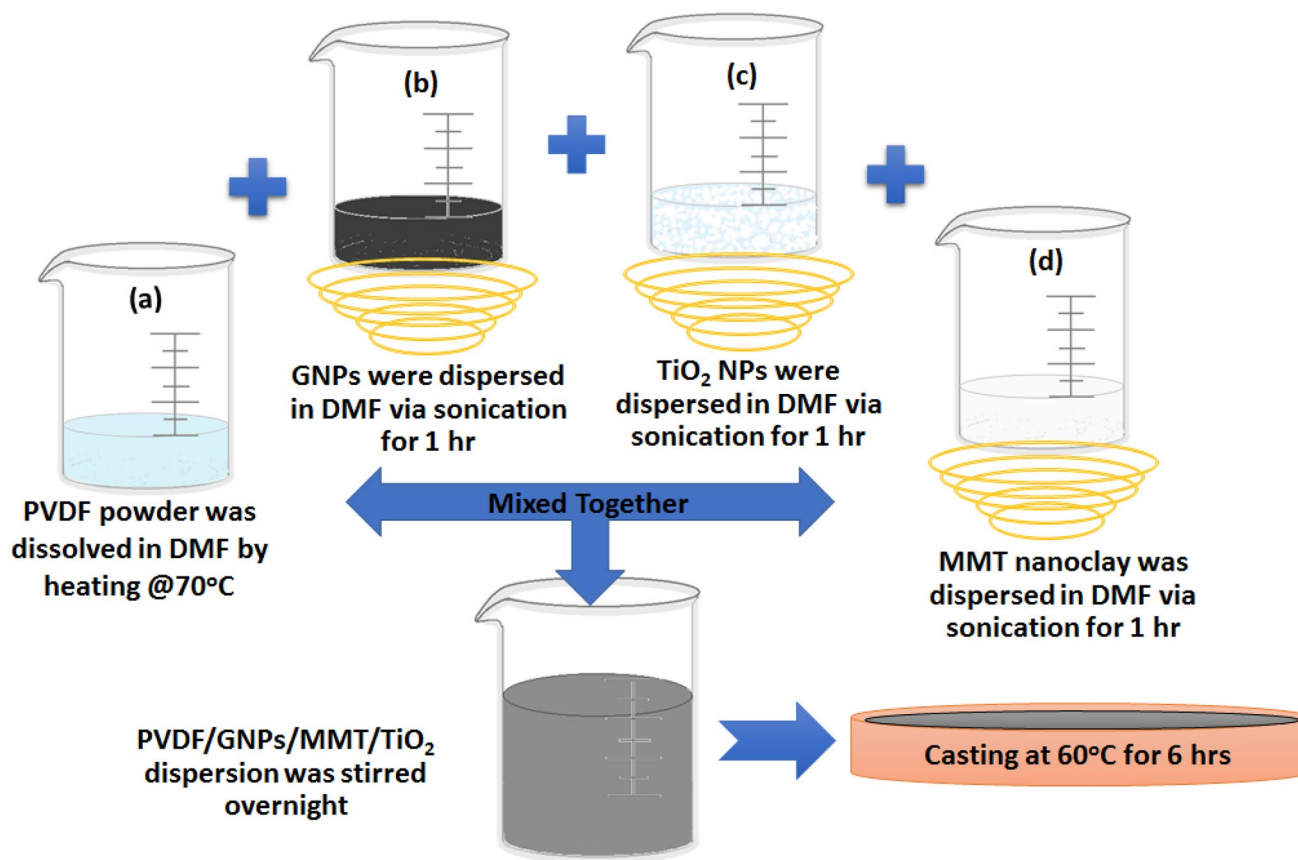


Fig. 1 Schematic representation of synthesis procedure

Table 1 Feed compositions of PVDF/GNPs/MMT/TiO₂ nanocomposite films

PVDF (wt%)	GNPs (wt%)	MMT (wt%)	TiO ₂ (wt%)
100	0	0	0
85	0.5	5	9.5
85	1	4	10
85	1.5	3	10.5
85	2	2	11
85	2.5	1	11.5
85	3	0	12

nanopowder was dispersed separately in 15 ml DMF by ultrasonication. The sonicated GNPs dispersion was then added to the PVDF solution followed by continuous stirring for 3 h. Likewise, the sonicated TiO₂ NPs and MMT nanoclay dispersions were respectively added to the PVDF/GNPs mixture. Later, the resulting PVDF/GNPs/MMT/TiO₂ mixture was stirred vigorously overnight at room temperature to obtain a homogeneous dispersion of nanofillers into the polymer matrix. Finally, the homogeneous PVDF/GNPs/MMT/TiO₂ dispersion was poured onto the Teflon

Petri dish and dried at 60 °C for 6 h to obtain PVDF/GNPs/MMT/TiO₂ nanocomposite films that were used for further characterizations.

2.3 Characterization Details

The FTIR spectra of pristine PVDF and PVDF/GNPs/MMT/TiO₂ nanocomposite films were obtained using Fourier transform infrared spectrophotometer (Shimadzu, IR Tracer-100, Japan) in the transmission mode within 400 to 4000 cm⁻¹ wavenumber range.

The XRD patterns of pristine PVDF, GNPs, MMT, TiO₂ NPs and PVDF/GNPs/MMT/TiO₂ nanocomposite films were taken using the X-ray source (Philips XPert MPD diffractometer, Eindhoven, The Netherlands) with Cu K α radiation of wavelength $\lambda = 1.5406 \text{ \AA}$ in the 2θ range from 10 to 80° with 1°/min scanning speed and 0.01° step size.

The surface morphology of PVDF/GNPs/MMT/TiO₂ nanocomposite films was evaluated using the field emission scanning electron microscope (FESEM; Tescan, MIRA3, Czech Republic) at different magnifications with an applied accelerating voltage of 20 kV.

Dielectric properties of the prepared PVDF/GNPs/MMT/TiO₂ nanocomposite films were studied using a frequency response impedance analyzer (N4L PSM 1735 NumetriQ, UK). The nanocomposite films were examined as a function of frequency ranging from 50 Hz to 20 MHz at different temperatures.

The EMI SE properties of PVDF and PVDF/GNPs/MMT/TiO₂ nanocomposite films were measured by using an 8510C vector network analyzer (VNA), Agilent Technologies, USA, in Ku-band (12–18 GHz) frequency region.

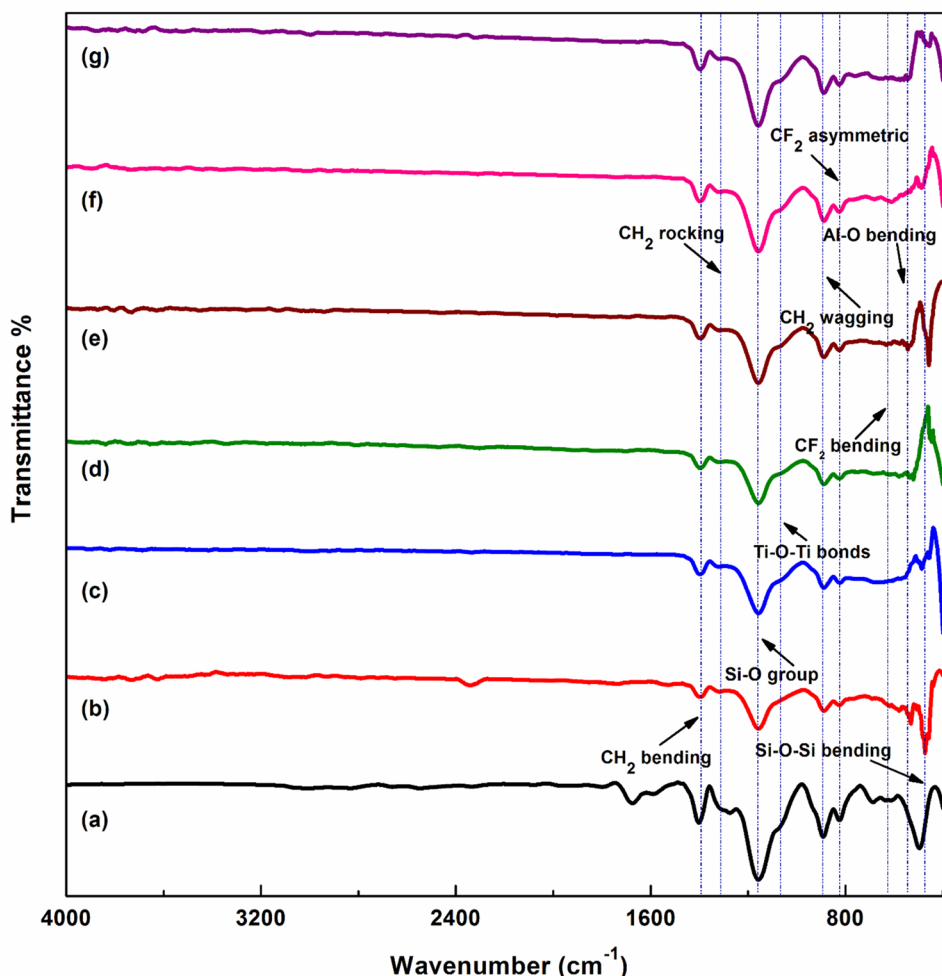
3 Results and Discussion

3.1 FTIR Spectroscopy

Figure 2 shows the FTIR transmittance spectra of pristine PVDF, PVDF/GNPs/MMT/TiO₂ and PVDF/GNPs/TiO₂ nanocomposite films for different content of GNPs, MMT and TiO₂ NPs into the PVDF matrix. In the FTIR spectrum of pristine PVDF (Fig. 2a), the small peaks at 3014 cm⁻¹

and 2978 cm⁻¹ are attributed to symmetric and asymmetric stretching vibrations of –CH₂ group respectively [29]. The peak at 1400 cm⁻¹ can be assigned to –CH₂ bending vibrations while the peaks at 1067, 1160 and 1400 cm⁻¹ show the presence of the α-PVDF phase [46]. The peak at 893 cm⁻¹ can be assigned to CH₂ rocking and CF₂ asymmetric stretching vibrations. Moreover, the peaks at 822, 893 and 1331 cm⁻¹ show the presence of the β-PVDF phase [52, 53]. The peaks around 621 cm⁻¹ can be assigned to –CF₂ bending while the peak at 490 cm⁻¹ can be attributed to –CF₂ bending and wagging vibrations [53]. The FTIR spectra of PVDF/GNPs/MMT/TiO₂ nanocomposites (Fig. 2b–g) show new peaks due to the incorporation of GNPs, MMT and TiO₂ NPs into the PVDF matrix. The peaks appearing at 1055 cm⁻¹ can be assigned to stretching vibrations of the Si–O group while the peaks at 540 cm⁻¹ and 473 cm⁻¹ are attributed to Al–O and Si–O–Si bending vibrations respectively. Also, the peak at 625 cm⁻¹ can be assigned for Al–O and Si–O out of plane vibrations of MMT [54]. The peaks for GNPs at 1067 and 1160 cm⁻¹ are merged with peaks of PVDF and the peak corresponding

Fig. 2 FTIR spectra of PVDF, PVDF/GNPs/MMT/TiO₂ and PVDF/GNPs/TiO₂ nanocomposite films (a) PVDF, (b) PVDF/GNPs/MMT/TiO₂ nanocomposite film with GNPs-0.5%, MMT-5% and TiO₂-9.5%, (c) GNPs-1%, MMT-4% and TiO₂-10%, (d) GNPs-1.5%, MMT-3% and TiO₂-10.5%, (e) GNPs-2%, MMT-2% and TiO₂-11%, (f) GNPs-2.5%, MMT-1% and TiO₂-11.5% and (g) GNPs-3% and TiO₂-12%



to the stretching vibrations of Ti–O–Ti bonds of TiO₂ NPs appears at 462 cm⁻¹ [46]. Therefore, the FTIR spectra of PVDF/GNPs/MMT/TiO₂ nanocomposites confirm the good interaction of nanofillers and the PVDF matrix.

3.2 XRD Analysis

The XRD patterns of pristine PVDF, TiO₂ NPs, GNPs and MMT nanoclay are shown in Fig. 3. The pristine PVDF showed a characteristic diffraction peak at $2\theta = 20.05^\circ$ which is attributed to the (110) crystal plane of α -phase while the second peak at $2\theta = 44.65^\circ$ is attributed to the (200) crystal plane of β -phase [21]. Besides, the diffraction pattern of PVDF also showed another prominent peak at $2\theta = 64.95^\circ$ which can be attributed to the (220) crystal plane [21]. The diffraction pattern of TiO₂ NPs showed several prominent XRD peaks at $2\theta = 25.24^\circ$ (101), $2\theta = 27.58^\circ$ (110), $2\theta = 37.98^\circ$ (004), $2\theta = 48.22^\circ$ (200), $2\theta = 53.98^\circ$ (105), $2\theta = 55.22^\circ$ (211), $2\theta = 62.76^\circ$ (204), $2\theta = 68.98^\circ$ (116), $2\theta = 70.36^\circ$ (220) and $2\theta = 75.28^\circ$ (215) which are

attributed to 80% anatase and 20% rutile crystallographic compositions [16]. The XRD pattern of GNPs showed a sharp and intense diffraction peak at $2\theta = 26.44^\circ$ and a small peak at $2\theta = 54.52^\circ$ demonstrating the highly crystalline graphite-like structure [55, 56]. The XRD pattern of MMT nanoclay also displayed several prominent diffraction peaks associated with its lamellar structure. The diffraction peak at $2\theta = 12.52^\circ$ is attributed to (001) reflection while the peaks at $2\theta = 20.62^\circ$ (100) and $2\theta = 35.08^\circ$ (110) are associated with pyrophyllite mineral phase of MMT [57, 58]. The XRD patterns of PVDF/GNPs/MMT/TiO₂ and PVDF/GNPs/TiO₂ nanocomposite films are depicted in Fig. 4. All the characteristics diffraction peaks of the polymer matrix and the nanofillers were observed in the XRD patterns of the nanocomposite films. However, the intensity of these XRD peaks in nanocomposites was lower as compared with the intensity of the XRD peaks of pristine components. This suggests good compatibility and strong interaction between the polymer matrix and the nanofillers that resulted in the formation of homogeneous nanocomposites.

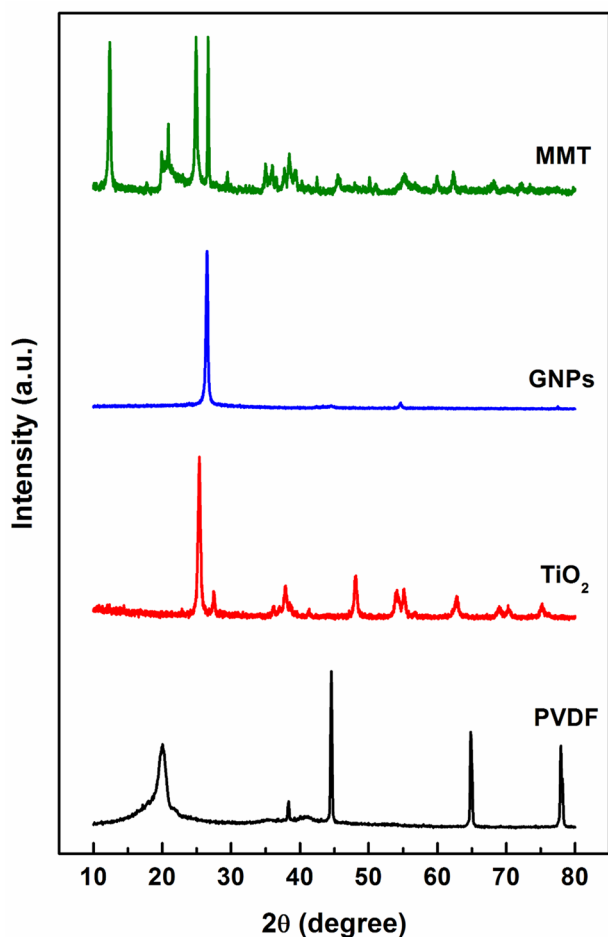


Fig. 3 XRD patterns of pristine PVDF, TiO₂ NPs, GNPs and MMT nanoclay

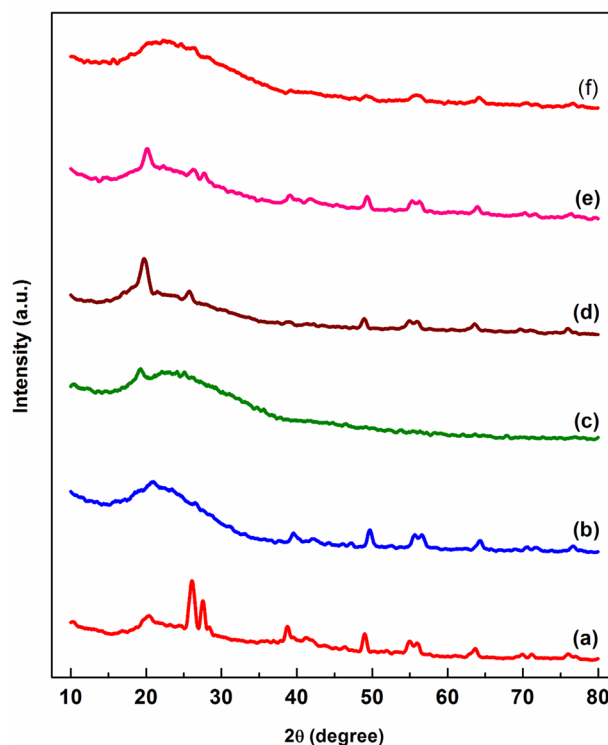


Fig. 4 XRD patterns of PVDF/GNPs/MMT/TiO₂ nanocomposite film with (a) GNPs-0.5%, MMT-5% and TiO₂-9.5%, (b) GNPs-1%, MMT-4% and TiO₂-10%, (c) GNPs-1.5%, MMT-3% and TiO₂-10.5%, (d) GNPs-2%, MMT-2% and TiO₂-11%, (e) GNPs-2.5%, MMT-1% and TiO₂-11.5%, and (f) PVDF/GNPs/TiO₂ nanocomposite film with GNPs-3% and TiO₂-12%

3.3 FESEM Analysis

Figure 5a–f shows FESEM images of three varied compositions of PVDF/GNPs/MMT/TiO₂ nanocomposite

films at different magnifications which revealed that the nanofillers i.e. GNPs, MMT and TiO₂ NPs are homogeneously dispersed within the PVDF matrix. The FESEM image of PVDF/GNPs/MMT/TiO₂ nanocomposite film

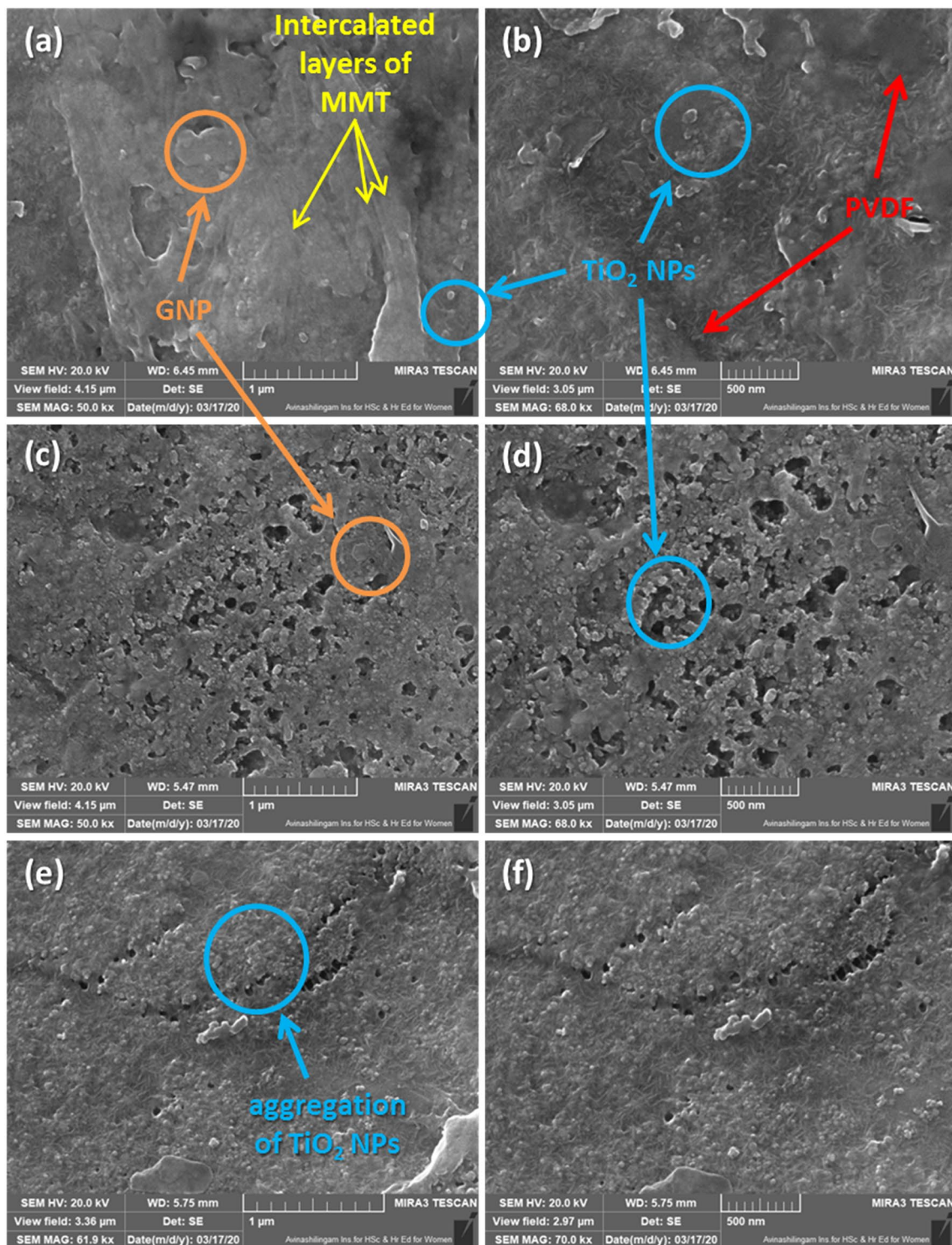


Fig. 5 a, b FESEM micrographs of PVDF/GNPs/MMT/TiO₂ nanocomposite film with GNPs-1%, MMT-4% and TiO₂-10% at different magnifications, c, d GNPs-2%, MMT-2% and TiO₂-11% at different magnifications and e, f GNPs-3% and TiO₂-12% at different magnifications

with GNPs-1%, MMT-4% and TiO₂-10% (Fig. 5a) shows randomly distributed intercalated layered stacks of MMT and also shows evenly distributed GNPs and TiO₂ NPs. On higher loading of GNPs and TiO₂ NPs with a decrease in MMT loading, the FESEM image of PVDF/GNPs/MMT/TiO₂ nanocomposite film with GNPs-2%, MMT-2% and TiO₂-11% (Fig. 5b) shows some aggregation of TiO₂ NPs with segregated GNPs. However, the little aggregation of TiO₂ NPs with the intercalated layers of MMT enhances the properties of the nanocomposites. On further increasing the TiO₂ NPs loading along with GNPs, the FESEM image of PVDF/GNPs/MMT/TiO₂ nanocomposite film with GNPs-2%, MMT-2% and TiO₂-11% (Fig. 5c) showed big aggregates of TiO₂ NPs. The FESEM micrographs of the nanocomposites demonstrates the uniform distribution of nanofillers throughout the PVDF matrix.

3.4 Dielectric Properties

In the present study, the dielectric properties of the prepared nanocomposite films were investigated and the dielectric constant was determined using the relation [59];

$$\epsilon = C_p t / \epsilon_0 A,$$

where C_p is capacitance, t is thickness of the film, ϵ_0 is permittivity of free space, A is area of the film.

Figure 6a–g shows the variation in dielectric constants for pristine PVDF and PVDF/GNPs/MMT/TiO₂ nanocomposite films as a function of frequency for various temperatures. The maximum value of the dielectric constant observed for pristine PVDF film was 47.11 at 50 Hz and 150 °C. On incorporating the nanofillers into the PVDF matrix, the

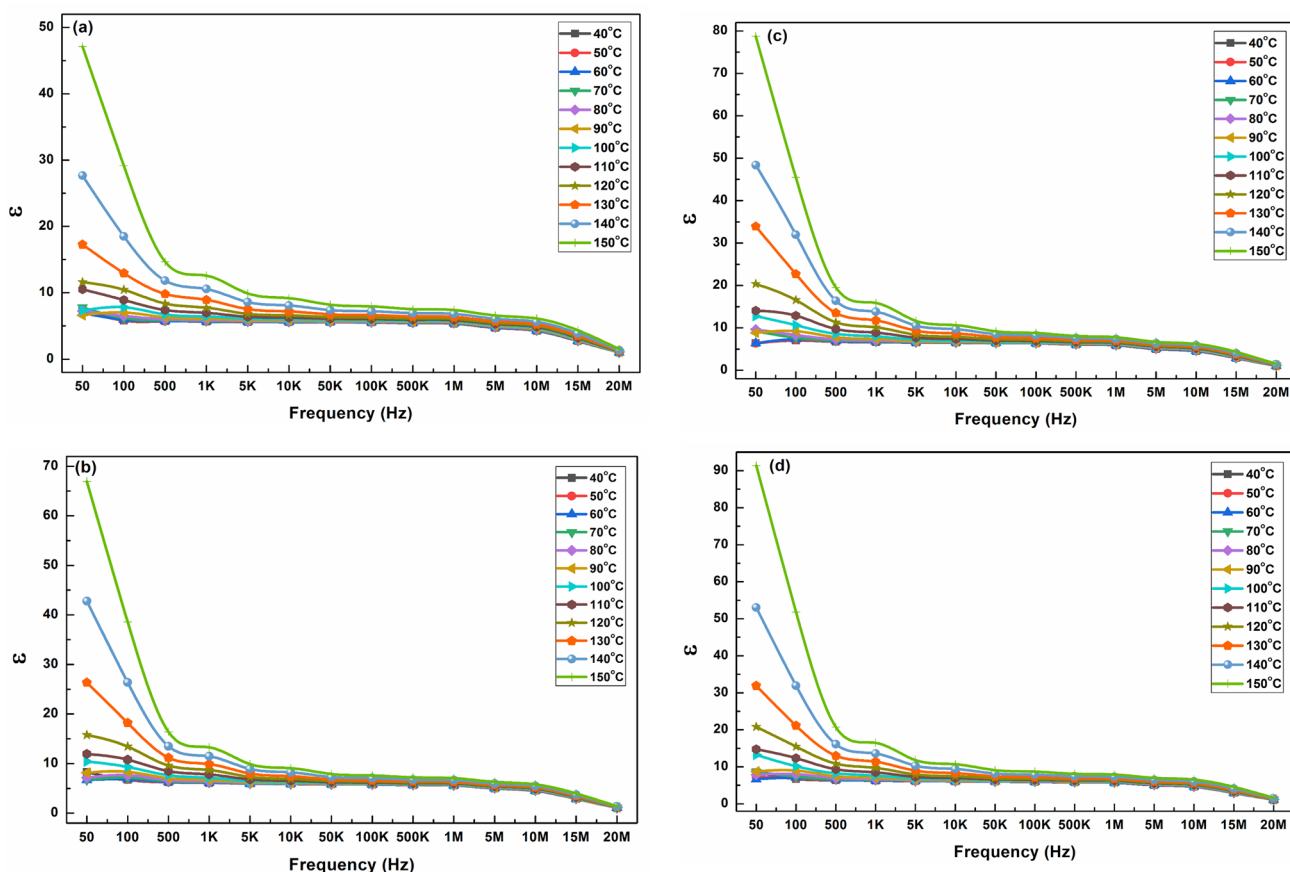


Fig. 6 **a** Dielectric constants for pristine PVDF film as a function of frequency at various temperatures. **b** Dielectric constants for PVDF/GNPs/MMT/TiO₂ nanocomposite film with GNPs-0.5%, MMT-5% and TiO₂-9.5% as a function of frequency at various temperatures. **c** Dielectric constants for PVDF/GNPs/MMT/TiO₂ nanocomposite film with GNPs-1%, MMT-4% and TiO₂-10% as a function of frequency at various temperatures. **d** Dielectric constants for PVDF/GNPs/MMT/TiO₂ nanocomposite film with GNPs-1.5%, MMT-3% and TiO₂-10.5% as a function of frequency at various temperatures.

e Dielectric constants for PVDF/GNPs/MMT/TiO₂ nanocomposite film with GNPs-2%, MMT-2% and TiO₂-11% as a function of frequency at various temperatures. **f** Dielectric constants for PVDF/GNPs/MMT/TiO₂ nanocomposite film with GNPs-2.5%, MMT-1% and TiO₂-11.5% as a function of frequency at various temperatures. **g** Dielectric constants for PVDF/GNPs/TiO₂ nanocomposite film with GNPs-3% and TiO₂-12% as a function of frequency at various temperatures

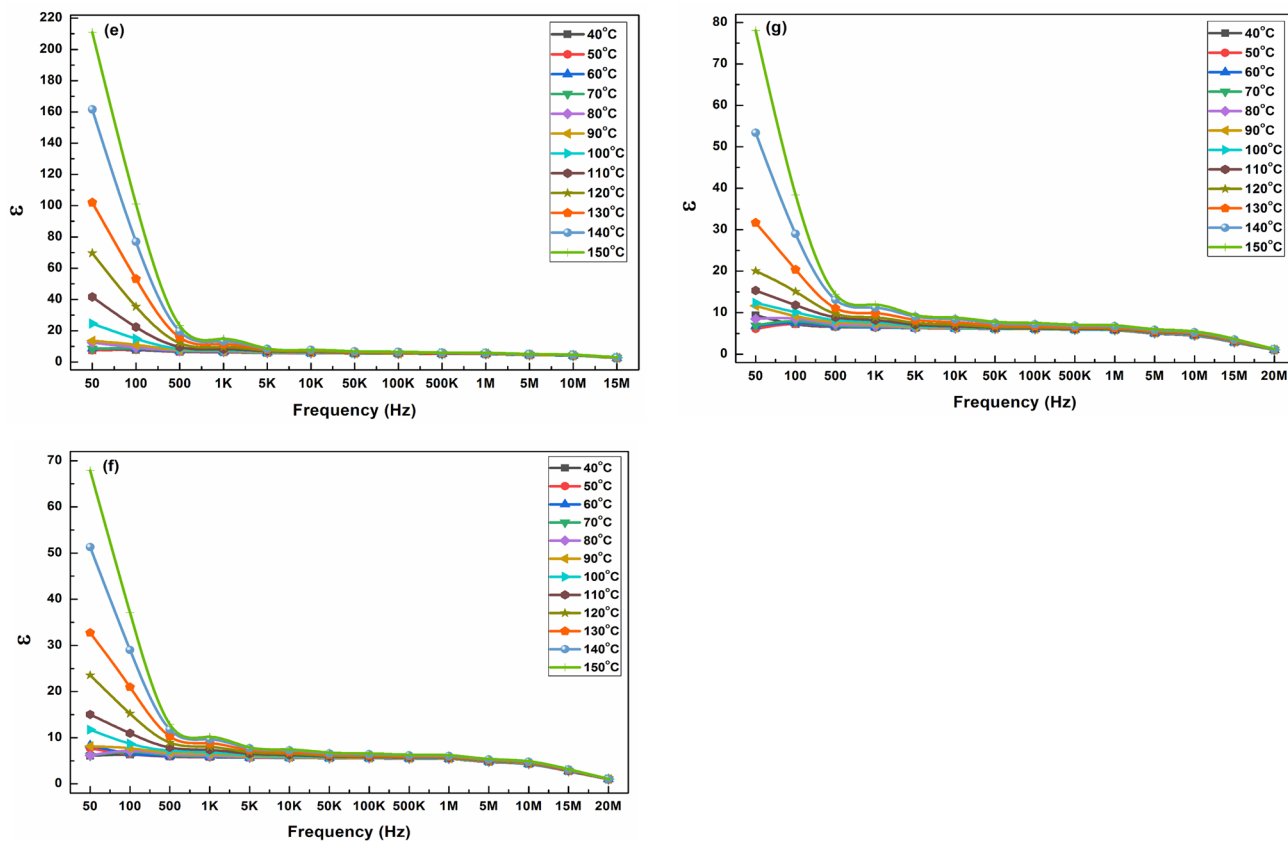


Fig. 6 (continued)

dielectric constant of the nanocomposites increased i.e. for PVDF/GNPs/MMT/TiO₂ nanocomposite film with GNPs-0.5%, MMT-5% and TiO₂-9.5%, the maximum dielectric constant value was found to be 66.94 at 50 Hz and at 150 °C. On higher loading of GNPs and TiO₂ NPs with decreasing MMT loading, the dielectric constant of the nanocomposites reached the maximum value of 210.92 at 50 Hz and at 150 °C for PVDF/GNPs/MMT/TiO₂ nanocomposite film with GNPs-2%, MMT-2% and TiO₂-11%. The high aspect ratio of GNPs and MMT effectively enhances the dielectric properties of the nanocomposites. Also, the fact that the addition of conducting fillers such as GNPs acts as electrodes and non-conducting counterparts as MMT and TiO₂ NPs act as a dielectric medium, when they are embedded into the polymer matrix forming microcapacitors [46]. It can be observed that all the nanocomposite films exhibit high dielectric constant values at low frequencies. When the frequency was increased, the dielectric constant decrease to very low values. This can be attributed to the interfacial polarization or Maxwell–Wagner–Sillars (MWS) effect [60], i.e. the dielectric constants are higher at lower frequencies

due to the induced and permanent dipoles which get aligned easily in this region. When the frequencies are higher, the dipoles have no time to get aligned, i.e., decreasing interfacial polarization or MWS effect [61]. On further increasing the concentration of GNPs and TiO₂ NPs and decreasing MMT loading, the dielectric constant values decrease. This can be due to the agglomeration of TiO₂ NPs and further settling down on GNPs that deteriorate the dielectric properties of the nanocomposites.

Dielectric loss is another important parameter of dielectric materials that results from the inability of the polarization to follow the rate of change of applied electric field. In general, the distortional, dipolar, interfacial, and conduction loss in the dielectric materials constitutes the dielectric loss of the material [60]. Figure 7a–g show the variations in the dielectric loss tangents for pristine PVDF and PVDF/GNPs/MMT/TiO₂ nanocomposite films as a function of frequency at various temperatures. The maximum value of dielectric loss tangent observed for pristine PVDF film was 5.4 at 50 Hz and 150 °C. For PVDF/GNPs/MMT/TiO₂ nanocomposite film with GNPs-2%, MMT-2% and TiO₂-11%, the maximum dielectric loss tangent value was found to be

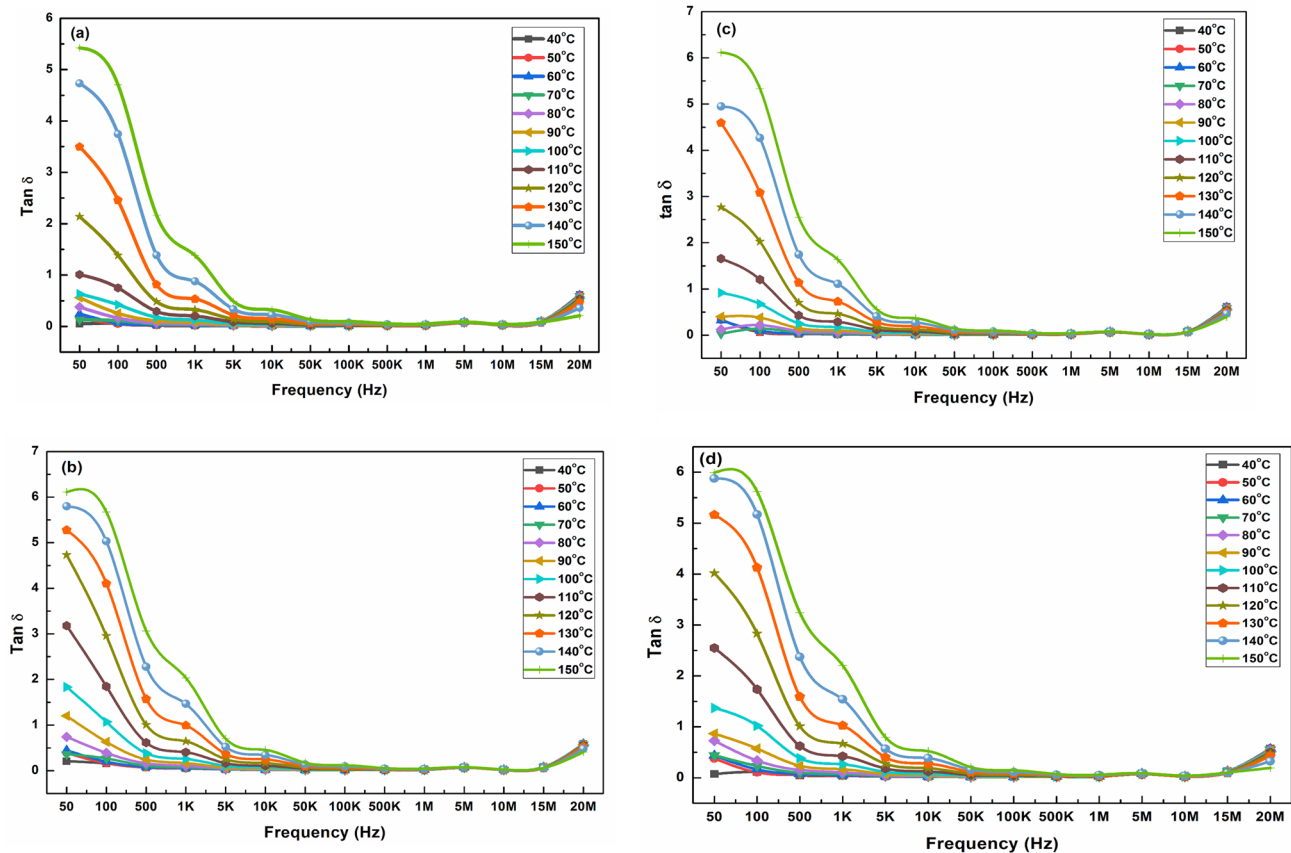


Fig. 7 **a** Dielectric loss tangents for pristine PVDF film as a function of frequency at various temperatures. **b** Dielectric loss tangents for PVDF/GNPs/MMT/TiO₂ nanocomposite film with GNPs-0.5%, MMT-5% and TiO₂-9.5% as a function of frequency at various temperatures. **c** Dielectric loss tangents for PVDF/GNPs/MMT/TiO₂ nanocomposite film with GNPs-1%, MMT-4% and TiO₂-10% as a function of frequency at various temperatures. **d** Dielectric loss tangents for PVDF/GNPs/MMT/TiO₂ nanocomposite film with GNPs-1.5%, MMT-3% and TiO₂-10.5% as a function of frequency at vari-

ous temperatures. **e** Dielectric loss tangents for PVDF/GNPs/MMT/TiO₂ nanocomposite film with GNPs-2%, MMT-2% and TiO₂-11% as a function of frequency at various temperatures. **f** Dielectric loss tangents for PVDF/GNPs/MMT/TiO₂ nanocomposite film with GNPs-2.5%, MMT-1% and TiO₂-11.5% as a function of frequency at various temperatures. **g** Dielectric loss tangents for PVDF/GNPs/TiO₂ nanocomposite film with GNPs-3% and TiO₂-12% as a function of frequency at various temperatures

10.4 at 50 Hz and 150 °C. This indicates that the addition of conducting GNPs into the polymer increases the conductivity of the nanocomposites which leads to the leakage of charge current causing an increase in loss tangent values [62, 63]. However, the dielectric constant values of all the nanocomposites are very much higher than their respective dielectric loss tangent values. This can be attributed to the good dispersion of nanofillers into the polymer matrix [60]. Table 2 gives the maximum dielectric constant and loss tangent values of the prepared nanocomposite films.

3.5 EMI SE

Figure 8 shows the EMI SE graph in the Ku band region for pristine PVDF and the PVDF/GNPs/MMT/TiO₂ nanocomposites. The pristine PVDF film shows EMI SE

of ~ 5.39 dB, which indicates its transparent shielding nature to EMI [4]. After the incorporation of nanofillers into the PVDF, the EMI SE raises to ~ 10.3 dB for PVDF/GNPs/MMT/TiO₂ nanocomposite film with GNPs-0.5%, MMT-5% and TiO₂-9.5%, then to ~ 11.5 dB for PVDF/GNPs/MMT/TiO₂ nanocomposite film with GNPs-2%, MMT-2% and TiO₂-11%. The maximum value of EMI SE attained for the prepared nanocomposites was ~ 12.6 dB for PVDF/GNPs/MMT/TiO₂ nanocomposite film with GNPs-2.5%, MMT-1% and TiO₂-11.5%. This increase in EMI SE can be attributed to the increased conductivity of nanocomposites due to the incorporation of GNPs. This shows that the GNPs form interconnected layers of conducting network and high specific surface area is provided by MMT and TiO₂ NPs. The effective enhancement in EMI SE can also be due to the attenuation in the scattering of

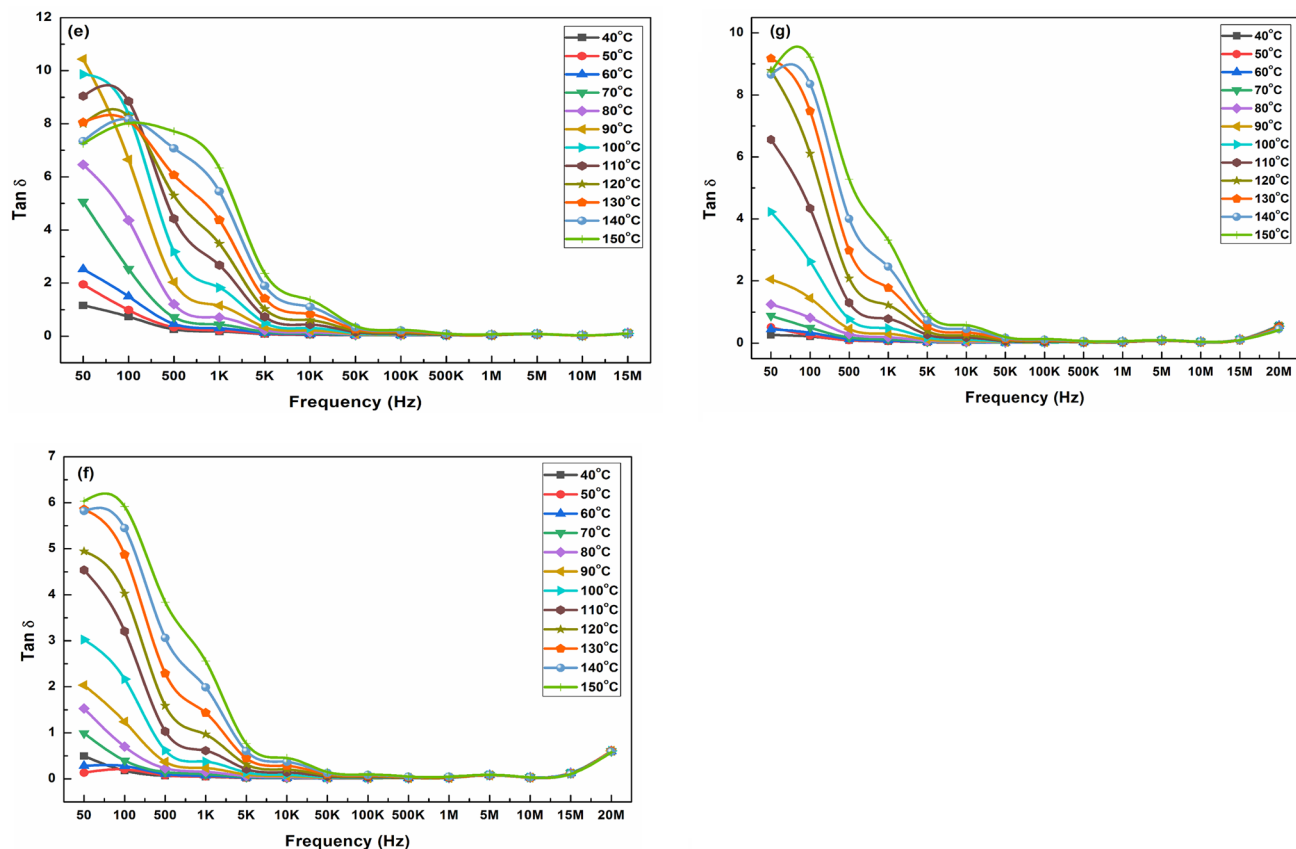


Fig. 7 (continued)

Table 2 Maximum dielectric constant and dielectric loss tangent values for PVDF/GNPs/MTM/TiO₂ nanocomposite films

Nanofiller loadings	Dielectric constant	Dielectric loss tangent
Pristine PVDF	47.11, 50 Hz, 150 °C	5.42, 50 Hz, 150 °C
GNPs-0.5%, MMT-5% and TiO ₂ -9.5%	66.94, 50 Hz, 150 °C	6.11, 50 Hz, 150 °C
GNPs-1%, MMT-4% and TiO ₂ -10%	78.74, 50 Hz, 150 °C	6.12, 50 Hz, 150 °C
GNPs-1.5%, MMT-3% and TiO ₂ -10.5%	91.36, 50 Hz, 150 °C	5.99, 50 Hz, 150 °C
GNPs-2%, MMT-2% and TiO ₂ -11%	210.92, 50 Hz, 150 °C	10.4, 50 Hz, 150 °C
GNPs-2.5%, MMT-1% and TiO ₂ -11.5%	67.88, 50 Hz, 150 °C	6.03, 50 Hz, 150 °C
GNPs-3%, and TiO ₂ -12%	78.09, 50 Hz, 150 °C	9.18, 50 Hz, 150 °C

EM waves using TiO₂ NPs [16]. The intercalated layers of MMT with its high aspect ratio along with GNPs i.e. flake or disc-like pieces play an effective role in absorbing the EM radiation [64]. Further enhancement of EMI SE can also be possible with increased loading of nanofillers into the PVDF matrix, but the mechanical stability of the resulting nanocomposite gets deteriorated on a higher concentration of fillers [8]. For the maximum loading of GNPs and TiO₂ NPs i.e., for PVDF/GNPs/TiO₂ nanocomposite

film with GNPs-3% and TiO₂-12%, the EMI SE value slightly decreases as compared with the lower loadings of GNPs and TiO₂ NPs. Table 3 depicts the literature survey for EMI SE of various PNCs [2, 5, 16, 23, 49, 64–66]. Therefore, with minimal incorporation of GNPs, MMT and TiO₂ NPs, a significant enhancement in EMI SE was observed which signifies that this nanocomposite material can be a potential candidate for EMI shielding application.

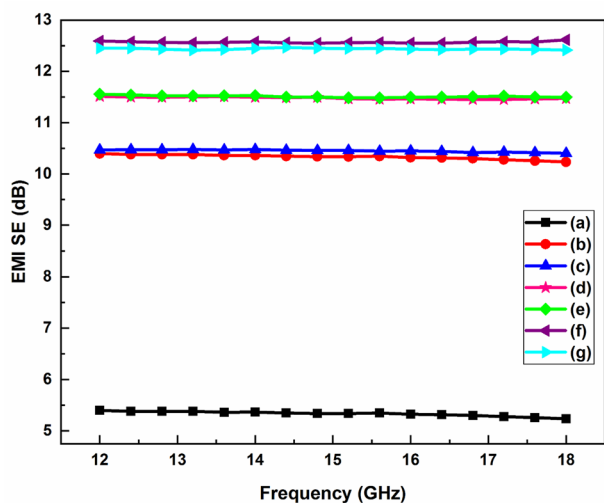


Fig. 8 EMI SE in the Ku band region for (a) pristine PVDF, (b) PVDF/GNPs/MMT/TiO₂ nanocomposite film with GNPs-0.5%, MMT-5% and TiO₂-9.5%, (c) GNPs-1%, MMT-4% and TiO₂-10%, (d) GNPs-1.5%, MMT-3% and TiO₂-10.5%, (e) GNPs-2%, MMT-2% and TiO₂-11%, (f) GNPs-2.5%, MMT-1% and TiO₂-11.5% and (g) GNPs-3% and TiO₂-12%

4 Conclusions

In the present work, PVDF/GNPs/MMT/TiO₂ nanocomposite films were successfully prepared using the solution casting method. The properties of prepared nanocomposites were investigated using different analysis techniques

such as FTIR, XRD, FESEM and dielectric analysis. The FTIR results infer good interaction between the nanofillers and the polymer matrix. FESEM micrographs demonstrate the homogenous dispersion of the nanofillers in the polymer matrix. The good interaction between the nanofillers and the polymer matrix with the homogeneous dispersion of the nanofillers within the polymer matrix led to the enhancement of the dielectric properties of the nanocomposites. The maximum dielectric constant of PVDF film was found to be 47.11 at 50 Hz, 150 °C and that of the PVDF/GNPs/MMT/TiO₂ nanocomposite film was observed to be 210.92 at 50 Hz, 150 °C for GNPs-2%, MMT-2% and TiO₂-11% loading. This value of the dielectric constant of nanocomposite film was 4.5 times greater than that of pristine PVDF film. On the other hand, the maximum dielectric loss tangent value was determined to be 10.4 at 50 Hz, 150 °C for the same compositions of the PVDF/GNPs/MMT/TiO₂ nanocomposite film which can be due to the increased conductivity of the nanocomposites. The maximum EMI SE of 12.6 dB was obtained in the Ku-band region for PVDF/GNPs/MMT/TiO₂ nanocomposites with GNPs-2.5%, MMT-1% and TiO₂-11.5% loading. The enhanced EMI SE values in the Ku-band frequency region can be attributed to the higher aspect ratio of nanofillers and the formation of conducting interconnected network between the nanofillers and the PVDF matrix. The obtained results suggest the potential of the prepared nanocomposites as an EMI shielding material.

Table 3 Summary of EMI SE values of various PNCs

Nanofillers	Loading (wt%)	Polymer matrix	Maximum EMI SE (dB)	Frequency (GHz)	References
h-BNNP	25	PVDF	11.21	8–12	[2]
NiO + WO ₃	20 + 5	PVC	12.05	8–12	[5]
TiO ₂	25	PVA/PSSA	13	8–12	[16]
MWCNTs + BaTiO ₃	3.7 + 7.5	PVDF-HFP-LiBF ₄	81	8–12	[23]
Graphene	15	PVDF	47	8–12	[49]
MMT	20	PPy	−32.63	8.6–12.4	[64]
rGO	2	Epoxy	38	0.5–4	[65]
GNPs	15	PLA	15.5	8–12	[66]
GNPs + MMT + TiO ₂	2.5 + 1 + 11.5	PVDF	12.6	8–12	This work

GNPs graphene nanoplatelets, rGO reduced graphene oxide, PVDF polyvinylidene fluoride, PLA polylactic acid, MMT montmorillonite, PPy polypyrrole, h-BNNP hexagonal boron nitride nanoparticles, TiO₂ titanium dioxide, PVA polyvinyl alcohol, PSSA polystyrene sulfonic acid, MWCNTs multiwalled carbon nanotubes, BaTiO₃ barium titanate, PVDF-HFP poly(vinylidene fluoride-co-hexafluoropropylene), LiBF₄ lithium tetrafluoroborate, NiO nickel oxide, WO₃ tungsten oxide, PVC polyvinyl chloride

Acknowledgement The authors Dr. M. Basheer Ahamed and A. Harish Kumar are very grateful to the Department of Science and Technology-Science and Engineering Research Board (DST-SERB), Government

of India, for providing the financial support to this research work under the sanctioned Project Number EMR/2016/006705.

References

- S. Sankaran, K. Deshmukh, M.B. Ahamed, S.K.K. Pasha, Recent advances in electromagnetic interference shielding properties of metal and carbon filler reinforced flexible polymer composites: a review. *Composites A* **114**, 49–71 (2018)
- S. Sankaran, K. Deshmukh, M.B. Ahamed, K.K. Sadasivuni, M. Faisal, S.K.K. Pasha, Electrical and Electromagnetic Interference (EMI) shielding properties of hexagonal boron nitride nanoparticles reinforced polyvinylidene fluoride nanocomposite films. *Polym. Plast. Technol. Mater.* **58**, 1191–1209 (2019)
- A. Muzaffar, M.B. Ahamed, K. Deshmukh, M. Faisal, Electromagnetic interference shielding properties of polyvinylchloride (PVC), barium titanate (BaTiO_3) and nickel oxide (NiO) based nanocomposites. *Polym. Test.* **77**, 105925 (2019)
- A. Muzaffar, M.B. Ahamed, K. Deshmukh, M. Faisal, S.K.K. Pasha, Enhanced electromagnetic absorption in NiO and BaTiO_3 based polyvinylidene fluoride nanocomposites. *Mater. Lett.* **218**, 217–220 (2018)
- A. Muzaffar, M.B. Ahamed, K. Deshmukh, S.K.K. Pasha, Dielectric properties and electromagnetic interference shielding studies of nickel oxide and tungsten oxide reinforced polyvinylchloride nanocomposites. *Polym. Plast. Technol. Mater.* **59**, 1667–1678 (2020)
- P. Rani, M.B. Ahamed, K. Deshmukh, Dielectric and electromagnetic interference shielding properties of carbon black nanoparticles reinforced PVA/PEG blend nanocomposite films. *Mater. Res. Express* **7**, 064008 (2020)
- J. Joseph, K. Deshmukh, K. Chidambaram, M. Faisal, E. Selvarajan, K.K. Sadasivuni, M.B. Ahamed, S.K.K. Pasha, Dielectric and electromagnetic interference shielding properties of germanium dioxide nanoparticle reinforced poly(vinyl chloride) and poly(methylmethacrylate) blend nanocomposites. *J. Mater. Sci. Mater. Electron.* **29**, 20172–20188 (2018)
- P. Rani, M.B. Ahamed, K. Deshmukh, Electromagnetic interference shielding properties of graphene quantum-dots reinforced poly(vinyl alcohol)/polypyrrole blend nanocomposites. *J. Appl. Polym. Sci.* **137**(45), 49392 (2020)
- P. Rani, M.B. Ahamed, K. Deshmukh, Significantly enhanced electromagnetic interference shielding effectiveness of monmorillonite nanoclay and copper oxide nanoparticles based polyvinylchloride nanocomposites. *Polym. Test.* **91**, 106744 (2020)
- L. Reddy, K. Deshmukh, T. Kovarik, D. Reiger, N.A. Nambiraj, R. Lakshmi pathy, S.K.K. Pasha, Enhanced dielectric properties of green synthesized nickel sulphide nanoparticles integrated polyvinyl alcohol nanocomposites. *Mater. Res. Express* **7**, 064007 (2020)
- K. Deshmukh, S.K.K. Pasha, Room temperature ammonia sensing based on graphene oxide integrated flexible polyvinylidene fluoride/cerium oxide nanocomposite films. *Polym. Plast. Technol. Mater.* **59**, 1429–1446 (2020)
- L. Reddy, K. Deshmukh, T. Kovarik, N.A. Nambiraj, S.K.K. Pasha, Green chemistry mediated synthesis of cadmium sulphide/polyvinylalcohol nanocomposites: assessment of microstructural, thermal and dielectric properties. *Polym. Compos.* **41**, 2054–2067 (2020)
- M.K. Mohanapriya, K. Deshmukh, K.K. Sadasivuni, G.J. Thangamani, K. Chidambaram, M.B. Ahamed, S.K.K. Pasha, Enhanced quality factor of polyvinyl formal (PVF) based nanocomposites filled with zinc oxide and carbon black nanoparticles for wireless sensing applications. *Mater. Today Proc.* **9**, 199–216 (2019)
- P.L. Reddy, K. Deshmukh, K. Chidambaram, M.B. Ahamed, K.K. Sadasivuni, D. Ponnamma, R. Lakshmi pathy, D. Dayananda, S.K.K. Pasha, Effect of polyethyleneglycol (PEG) on structural, thermal and photoluminescence properties of CdO nanoparticles for optoelectronic applications. *Mater. Today Proc.* **9**, 175–183 (2019)
- P.L. Reddy, K. Deshmukh, K. Chidambaram, M.M. Nazir Ali, K.K. Sadasivuni, Y. Ravi Kumar, R. Lakshmi pathy, S.K.K. Pasha, Dielectric properties of polyvinyl alcohol (PVA) nanocomposites filled with green synthesized zinc sulphide (ZnS) nanoparticles. *J. Mater. Sci. Mater. Electron.* **30**, 4676–4687 (2019)
- M.K. Mohanapriya, K. Deshmukh, J. Kadlec, K.K. Sadasivuni, M. Faisal, N.A. Nambiraj, S.K.K. Pasha, Dynamic mechanical analysis and broadband electromagnetic interference shielding characteristics of poly (vinyl alcohol)–poly (4-styrenesulfonic acid)–titanium dioxide nanoparticles based tertiary nanocomposites. *Polym. Plast. Technol. Mater.* **59**, 847–863 (2019)
- Y.R. Kumar, K. Deshmukh, K.K. Sadasivuni, S.K.K. Pasha, Graphene quantum dots based materials for sensing, bioimaging and energy storage applications: a review. *RSC Adv.* **10**, 23861–23898 (2020)
- R.S. Dongre, K.K. Sadasivuni, K. Deshmukh, A. Mehta, S. Basu, J.S. Meshram, M.A.A. Al-Maadeed, A. Karim, Natural polymer based composite membranes for water purification: a review. *Polym. Plast. Technol. Mater.* **58**, 1295–1310 (2019)
- K.K. Sadasivuni, J.J. Cabibihan, K. Deshmukh, S. Gautham, M.K. Abubasha, J.P. Gogoi, I. Klemenoks, G. Sakale, B.S. Sekhar, P.S.R. Sreekanth, K.V. Rao, M. Knite, A review on porous polymer composite materials for multifunctional electronic applications. *Polym. Plast. Technol. Mater.* **58**, 1253–1294 (2019)
- H. Aghamohammadi, R. Eslami-Farsani, A. Tcharkhtchi, The effect of multi-walled carbon nanotubes on the mechanical behavior of basalt fibers metal laminates: an experimental study. *Int. J. Adhes. Adhes.* **98**, 102538 (2020)
- P. Rani, M.B. Ahamed, K. Deshmukh, Dielectric and electromagnetic interference shielding properties of zeolite 13X and carbon black nanoparticles based PVDF nanocomposites. *J. Appl. Polym. Sci.* (2020). <https://doi.org/10.1002/app.50107>
- P. Rani, M.B. Ahamed, K. Deshmukh, Structural, dielectric and EMI shielding properties of polyvinyl alcohol/chitosan blend nanocomposites integrated with graphite oxide and nickel oxide nanofillers. *J. Mater. Sci. Mater. Electron.* (2020). <https://doi.org/10.1007/s10854-020-04855-w>
- M.K. Vyas, A. Chandra, Synergistic effect of conducting and insulating fillers in polymer nanocomposite films for attenuation of X-band. *J. Mater. Sci.* **54**, 1304–1325 (2019)
- S.K. Sharma, V. Gupta, R.P. Tandon, V.K. Sachdev, Synergistic effect of graphene and MWCNT fillers on electromagnetic shielding properties of graphene–MWCNT/ABS nanocomposites. *RSC Adv.* **6**, 18257–18265 (2016)
- S.M. Pawde, K. Deshmukh, Studies on surface properties of polymeric coated paper material. *J. Appl. Polym. Sci.* **101**, 4167–4171 (2006)
- S.M. Pawde, K. Deshmukh, Surface characterization of air plasma treated polyvinylidene fluoride and polymethylmethacrylate films. *Polym. Eng. Sci.* **49**, 808–811 (2009)
- S.M. Pawde, K. Deshmukh, Investigation of the structural, thermal, mechanical and optical properties of poly(methylmethacrylate) and poly (vinylidene fluoride) blends. *J. Appl. Polym. Sci.* **114**, 2169–2179 (2009)
- K. Deshmukh, G.M. Joshi, Novel nanocomposites of graphene oxide reinforced poly (3,

- 4-ethylenedioxythiophene)-block-poly(ethyleneglycol) and polyvinylidene fluoride for embedded capacitor. *RSC Adv.* **4**, 37954–37963 (2014)
29. D. Satapathy, K. Deshmukh, M.B. Ahamed, K.K. Sadasivuni, D. Ponnamma, S.K.K. Pasha, M.A.A. AlMaadeed, J. Ahmad, High-quality factor poly (vinylidene fluoride) based novel nanocomposites filled with graphene nanoplatelets and vanadium pentoxide for high-Q capacitor applications. *Adv. Mater. Lett.* **8**, 288–294 (2017)
 30. K. Deshmukh, M.B. Ahamed, R.R. Deshmukh, S.K.K. Pasha, K.K. Sadasivuni, D. Ponnamma, M.A.A. AlMaadeed, Striking multiple synergies in novel three-phase fluoropolymer nanocomposites by combining titanium dioxide and graphene oxide as hybrid fillers. *J. Mater. Sci. Mater. Electron.* **28**, 559–575 (2016)
 31. H. Aghamohammadi, R. Eslami-Farsani, M. Torabian, N. Amousa, Recent advances in one-pot functionalization of graphene using electrochemical exfoliation of graphite: a review. *Synth. Met.* **269**, 116549 (2020)
 32. K. Deshmukh, S.M. Khatake, G.M. Joshi, Surface properties of graphene oxide reinforced polyvinylchloride nanocomposites. *J. Polym. Res.* **20**, 286 (2013)
 33. W.K. Chee, H.N. Lim, Z. Zainal, N.M. Huang, I. Harrison, Y. Andou, Flexible graphene-based supercapacitors: a review. *J. Phys. Chem. C* **120**, 4153–4172 (2016)
 34. H.J. Choi, S.M. Jung, J.M. Seo, D.W. Chang, L. Dai, J.B. Baek, Graphene for energy conversion and storage in fuel cells and supercapacitors. *Nano Energy* **1**, 534–551 (2012)
 35. F. Bonaccorso, Z. Sun, T. Hasan, A.C. Ferrari, Graphene photonics and optoelectronics. *Nat. Photonics* **4**, 611–622 (2010)
 36. G. Wang, X. Shen, J. Yao, J. Park, Graphene nanosheets for enhanced lithium storage in lithium ion batteries. *Carbon* **47**, 2049–2053 (2009)
 37. P. Cataldi, A. Athanassiou, I.S. Bayer, Graphene nanoplatelets-based advanced materials and recent progress in sustainable applications. *Appl. Sci.* **8**, 1438 (2018)
 38. I. Mutlay, L.B. Tudoran, Percolation behavior of electrically conductive graphene nanoplatelets/polymer nanocomposites: theory and experiment. *Fuller. Nanotubes Carbon Nanostruct.* **22**, 413–433 (2014)
 39. R. Keshavarz, H. Aghamohammadi, R. Eslami-Farsani, The effect of graphene nanoplatelets on the flexural properties of fiber metal laminates under marine environmental condition. *Int. J. Adhes. Adhes.* **103**, 102709 (2020)
 40. E. Kazemi-Khasragh, F. Bahari-Sambran, C. Platzter, R. Eslami-Farsani, The synergistic effect of graphene nanoplatelets–montmorillonite hybrid system on the tribological behaviour of epoxy-based nanocomposites. *Tribol. Int.* **151**, 106472 (2020)
 41. Y. Li, S.C. Tjong, Electrical properties of binary PVDF/clay and ternary graphite-doped PVDF/clay nanocomposites. *Curr. Nanosci.* **8**, 732–738 (2012)
 42. Q.Y. Peng, P.H. Cong, X.J. Liu, T.X. Liu, S. Huang, T.S. Li, The preparation of PVDF/clay nanocomposites and the investigation of their tribological properties. *Wear* **266**, 713–720 (2009)
 43. W. Yu, Z. Zhao, W. Zheng, Y. Song, B. Li, B. Long, Q. Jiang, Structural characteristics of poly (vinylidene fluoride)/clay nanocomposites. *Mater. Lett.* **62**, 747–750 (2008)
 44. J. Ahmad, K. Deshmukh, M.B. Hägg, Influence of TiO₂ on the chemical, mechanical, and gas separation properties of polyvinyl alcohol–titanium dioxide (PVA–TiO₂) nanocomposite membranes. *Int. J. Polym. Anal. Charact.* **18**, 287–296 (2013)
 45. K. Deshmukh, J. Ahmad, G.M. Joshi, M.B. Ahamed, M.B. Hägg, Stability and electrokinetic properties of aqueous TiO₂ nanoparticle dispersion in polyallylamine and polyvinylalcohol blend systems. *Int. J. Polym. Res.* **21**, 393 (2014)
 46. S. Ishaq, F. Kanwal, S. Atiq, M. Moussa, U. Azhar, D. Losic, Dielectric properties of graphene/titania/polyvinylidene fluoride (G/TiO₂/PVDF) nanocomposites. *Materials* **13**, 205 (2020)
 47. D.Y. Wang, Y.P. Song, J.S. Wang, X.G. Ge, Y.Z. Wang, A.A. Stec, T.R. Hull, Double In situ approach for the preparation of polymer nanocomposite with multi-functionality. *Nanoscale Res. Lett.* **4**, 303–306 (2009)
 48. G. Polizos, E. Tuncer, I. Sauers, K.L. More, Physical properties of epoxy resin/titanium dioxide nanocomposites. *J. Polym. Eng. Sci* **51**, 87–93 (2011)
 49. K. Sabira, M.P. Jayakrishnan, P. Saheeda, S. Jayalekshmi, On the absorption dominated EMI shielding effects in free standing and flexible films of poly(vinylidene fluoride)/graphene nanocomposite. *Eur. Polym. J.* **99**, 437–444 (2018)
 50. M. Hamidinejad, B. Zhao, A. Zandieh, N. Moghimi, T. Filleter, C.B. Park, Enhanced electrical and electromagnetic interference shielding properties of polymer–graphene nanoplatelet composites fabricated via supercritical-fluid treatment and physical foaming. *ACS Appl. Mater. Interfaces* **10**, 30752–30761 (2018)
 51. J.M. Thomassin, C. Jérôme, T. Pardoën, C. Bailly, I. Huynen, C. Detrembleur, Polymer/carbon based composites as electromagnetic interference (EMI) shielding materials. *Mater. Sci. Eng. R* **74**, 211–232 (2013)
 52. A. Salimi, A.A. Yousefi, FTIR studies of β -phase crystal formation in stretched PVDF films. *Polym. Test.* **22**, 699–704 (2003)
 53. A.S. Lanceros-Mendez, J.F. Mano, V.H. Schmidt, FTIR and DSC studies of mechanically deformed β -PVDF films. *J. Macromol. Sci.* **527**, 517–527 (2001)
 54. P. Taylor, Z. Danková, A. Mockov, S. Dolinská, Z. Dankova, Desalination and water treatment influence of ultrasound irradiation on cadmium cations adsorption by montmorillonite. *Desalin. Water Treat.* **52**, 5462–5469 (2014)
 55. C. Zhang, L. Zhong, D. Wang, F. Zhang, G. Zhang, Anti-ultraviolet and anti-static modification of polyethylene terephthalate fabrics with graphene nanoplatelets by a high-temperature and high-pressure inlaying method. *Text. Res. J.* **89**, 1488–1499 (2018)
 56. Y. Wang, J. Yang, K. Du, Q. Yin, Q. Yin, Polypyrrole/graphene/polyaniline ternary nanocomposite with high thermoelectric power factor. *ACS Appl. Mater. Interfaces* **9**, 20124–20131 (2017)
 57. N. Ahmad, S.T. Hussain, B. Muhammad, N. Ali, S.M. Abbas, Y. Khan, Effect of manganese promotion on Al-pillared montmorillonite supported cobalt nanoparticles for Fischer-Tropsch synthesis. *Bull. Korean Chem. Soc.* **34**, 3005–3012 (2013)
 58. C.R. Silva, R.M. Lago, H.S. Veloso, P.S.O. Patrisio, Use of amphiphilic composites based on clay/carbon nanofibers as fillers in UHMWPE. *J. Braz. Chem. Soc.* **29**, 278–284 (2018)
 59. D. Ponnamma, H. Parangusan, K. Deshmukh, P. Kar, A. Muzaffar, S.K.K. Pasha, M.B. Ahamed, M.A.A. AlMaadeed, Green synthesized materials for sensor, actuator, energy storage and energy generation: a review. *Polym. Plast. Technol. Mater.* **59**, 1–62 (2020)
 60. K. Deshmukh, M.B. Ahamed, K.K. Sadasivuni, D. Ponnamma, R.R. Deshmukh, S.K.K. Pasha, M.A.A. AlMaadeed, K. Chidambaram, Graphene oxide reinforced polyvinyl alcohol/polyethylene glycol blend composites as high-performance dielectric material. *J. Polym. Res.* **23**, 159 (2016)
 61. K. Deshmukh, S. Sankaran, M.B. Ahamed, K.K. Sadasivuni, S.K.K. Pasha, D. Ponnamma, P.S.R. Sreekanth, K. Chidambaram, Dielectric Spectroscopy. In: *Spectroscopic Methods for Nanomaterial Characterization: Micro and Nano Technologies* (Elsevier, Amsterdam, 2017), pp. 237–299
 62. K. Deshmukh, M.B. Ahamed, S. Sankaran, S.K.K. Pasha, K.K. Sadasivuni, D. Ponnamma, M.A.A. AlMaadeed, Studies on the mechanical, morphological and electrical properties of highly dispersible graphene oxide reinforced polypyrrole and polyvinyl

- alcohol blend composites. *Mater. Today Proc.* **5**, 8744–8752 (2018)
63. K. Deshmukh, S. Sankaran, M.B. Ahamed, S.K.K. Pasha, K.K. Sadasivuni, D. Ponnamma, M.A.A. AlMaadeed, K. Chidambaram, Studies on the electrical properties of graphene oxide-reinforced poly (4-styrene sulfonic acid) and polyvinyl alcohol blend composites. *Int. J. Nanosci.* **17**, 1760005–1760013 (2017)
64. J. Jin, J. Song, S. Deng, G. Li, Synthesis and microwave absorbing characteristics of flake-like polypyrrole filled composites in X-band. *Polym. Compos.* **37**, 532–538 (2014)
65. N. Yousefi, X. Sun, X. Lin, X. Shen, J. Jia, B. Zhang, B. Tang, M. Chan, J.K. Kim, Highly aligned graphene/polymer nanocomposites with excellent dielectric properties for high-performance electromagnetic interference shielding. *Adv. Mater.* **26**, 5480–5487 (2014)
66. S. Kashi, R.K. Gupta, T. Baum, N. Kao, S.N. Bhattacharya, Morphology, electromagnetic properties and electromagnetic interference shielding performance of poly lactide/graphene nanoplatelet nanocomposites. *Mater. Des.* **95**, 119–126 (2016)

Publisher's Note Springer Nature remains neutral with regard to jurisdictional claims in published maps and institutional affiliations.